

# Selective catalysis for the reductive amination of furfural towards furfurylamine by the graphene-co-shelled cobalt nanoparticles

Xiuzheng Zhuang<sup>1, 2#</sup>, Jianguo Liu<sup>1, 3\*#</sup>, Shurong Zhong<sup>1</sup>, Longlong Ma<sup>1\*</sup>

1 CAS Key Laboratory of Renewable Energy, Guangdong Provincial Key Laboratory of New and Renewable Energy Research and Development, Guangzhou Institute of Energy Conversion, Chinese Academy of Sciences, Guangzhou 510640, P. R. China.

2 University of Chinese Academy of Sciences, Beijing 100049, P. R. China.

3 Dalian National Laboratory for Clean Energy, Dalian 116023, P. R. China.

\* Corresponding authors e-mail: liujg@ms.giec.ac.cn; mall@ms.giec.ac.cn

# These authors contributed equally to this work.

Abstract: Amines with functional groups are widely used in the manufacture of pharmaceuticals, agricultural chemicals, polymers, and surfactants; so far, amines are mostly produced via petrochemical routes, which motivates the sustainable production of amines from renewable resources, such as biomass. Unfortunately, the reductive amination of biomass-derived platforms is now suffering from challenges, e.g. poor selectivity and carbon balances, because of the restriction of homogenous catalyst. For this reason, we developed an eco-friendly, simplified, and highly effective procedure for the preparation of non-toxic heterogeneous catalyst based on the earth-abundant metals (i.e., cobalt), whose catalytic activity on furfural or other biomass-derived platforms were proved to be broadly available. The corresponding conversion rate and few of side products were also determined so as to optimized the reaction conditions, suggesting that the prepared cobalt-supported catalyst enables easy substitution of  $-NH_2$  moiety towards functionalized and structurally diverse molecules, even under very mild industrially viable and scalable conditions. More surprisingly, the cobalt-supported catalyst could also be expediently recycled by magnetic bar and still remained the excellent catalytic activity after reusing up to eight times; on another hands, the gram-scale reductive amination catalyzed by the same catalyst exhibited the similar yield of target products in comparison to its smaller scale, which was comparable to the reported heterogeneous noble-based catalysts. And also, results from a series of analytic technologies involving XRD, XPS, TEM/Mapping and *in-suit* FTIR revealed that the structural features of catalyst are closely in relation to its catalytic mechanisms; in simple terms, the outer graphitic shell is activated by the electronic interaction between the inner metallic nanoparticles and the carbon layer as well as the induced charge redistribution. In conclusion, this newly developed catalysts enable the synthesis of amines from biomass-derived platforms with satisfied selectivity and carbon balance, providing a cost-effective and sustainable access to the widely application of reductive amination.

## 1. Introduction

Interest in the development of sustainable chemistry is continuously growing towards producing valuable chemicals and fuels from renewable resource given the expected shortage of fossil-based resources<sup>1,2</sup>. In this regard, lignocellulosic biomass stands out as a promising renewable carbon source for chemical industry because of its advantages on abundant reserves, eco-friendliness, and worldwide distribution<sup>3-5</sup>. As we already known, the transformation of lignocellulosic components (i.e., hemicellulose, cellulose, and lignin) into small organic intermediates, namely platform molecules, is the essential precursors to progress towards the synthesis of fine chemicals, drop-in biofuels, and biodegradable materials<sup>6</sup>. So far, a variety of platform molecules, including but not limited to furfural, 5-hydroxymethylfurfural (5-HMF), levulinic acid and phenol (or phenol derives), can be easily obtained from lignocellulosic biomass, which can be used as substitutes for fossil-based feedstock in the manufacture of valuable compounds, especially in the field of fine chemicals<sup>7-9</sup>. One of the acceptable strategy for the synthesis of high-value chemicals is related to the reductive amination which is superior in terms of its high selectivity towards targeted N-containing components, its availability under very mild conditions, and its diversity in product compounds<sup>10</sup>, motivating the increase of academic attentions in the reductive amination of biomass-derived platforms in the recent years. Among these platform molecules, furfural is easily accessible from acid-catalyzed tandem hydrolysis dehydration of hemicellulose or from acid-facilitated transformation of cellulose-derived hexoses, exhibiting an attractive economic benefit when compared to other biomass-derived platform<sup>11,12</sup>. In general, furfural can be reacted with ammonia or primary amines to synthesize valuable amines, such as furfurylamine and its derivatives, which have a large spectrum of application in the manufacture of pharmaceuticals, pesticides, synthetic resins, and useful agrochemicals. As reported by Mariscal et al.<sup>13</sup>, reductive amination of furfural with amines or ammonia is a kind of cascade reaction consisting of the formation of imines and sequential hydrogenation to produce furfurylamine or its derivatives, and the key step during this process is the selective hydrogenation of in-situ formed imines to amines owing to the presence of competitive side reaction<sup>14</sup>. In this reaction network depicted in Fig.1, furfural can be hydrogenated to the alcohol (step A), react with ammonia to form reactive intermediates, or react with the target product (i.e., furfurylamine) to form the secondary imine (step B). It is worthwhile that there are still minor mechanistic details under debate surrounding the condensation reaction in step B, which was discussed extensively in a thorough review by Gomez et al.<sup>15</sup> Once the secondary imine is formed, it was easily hydrogenated to the secondary amine (step C) that can be further condensed with furfurylamine as step B, or it can be decomposed to the primary imine (or amine) in the presence of ammonia (step D). And also, the primary imine can also be hydrogenated to the target amine in step E. Unfavorable side reactions involve the formation of difurfurylamine and furfuryl alcohol competing with the formation of furfurylamine

rendering the selectivity synthesis of furfurylamine challenging<sup>6</sup>. This was further corroborated by Hara et al.<sup>16</sup> by means of density functional theory (DFT) calculations, suggesting that the formation of difurfurylamine and furfuryl alcohol was more thermodynamically favorable relative to the formation of furfurylamine. As the result, the competition between main and side reaction is the main to cause the carbon loss of target product, and thus seeking the suitable catalysts to regulate the reaction balance is of important for the sustainable synthesis of functional amines from biomass-derived platforms.

A series of noble metal-based catalysts have been developed for the reductive amination of furfural using ammonia as nitrogen source and H<sub>2</sub> as reductant, and the details are described in Fig,1. For instance, with the help of homogeneous RuCl<sub>2</sub>(PPh<sub>3</sub>)<sub>3</sub> as catalyst, Jagadeesh et al.<sup>17, 18</sup> yielded 85 % furfurylamine from the reductive amination of furfural under 130 °C, 24 h and 4 MPa H<sub>2</sub>, but the difficulties in separation and reuse limits its practical applications. Exploitation of heterogeneous catalysts for the reductive amination of furfural has thus become focus of research. Ebitani and co-workers<sup>19</sup> indicated that the Ru-based catalyst supported by hydroxyapatite (Ru-PVP/HAP) facilitated reductive amination of furfural and afforded a relatively lower yield of furfurylamine at 60 %, similar with other Ru-based oxide-supported catalyst reported by Chatterjee et al.<sup>14</sup> and Komanoya et al.<sup>16</sup> The unfavorable side reactions included the formation of difurfurylamine and furfuryl alcohol are the major reaction which challenges the reductive amination of furfural, while Martinez et al.<sup>20</sup> found that screening and adjusting the structural features of supports is beneficial for selectivity synthesis owing to the synergistic effect of acid sites and metal sites. On another hands, the expensive and scarcity of noble metal-based catalysts arise negative effects on the production cost as well as its large-scale application, which motivates the low-cost and abundant non-noble metal-based catalysts for the reductive amination of furfural<sup>6</sup>. Xu and co-workers<sup>21</sup> indicated that both of the commercial Raney Ni and Raney Co enabled the reductive amination of furfural with ammonia to proceed well, but the latter was proved to be superior to the former in terms of higher selectivity towards furfurylamine as the metallic cobalt facilitates hydrogenolysis of N-furfurylidene-furfurylamine. Additionally, Varma et al.<sup>22</sup> prepared a magnetic Fe<sub>3</sub>O<sub>4</sub>@SiO<sub>2</sub>-Ni catalyst with core-shell structure for the reductive amination of furfural in ammonia solution under 115 °C, 2 h and 2 MPa H<sub>2</sub>, which yield 73 % furfurylamine but meanwhile exhibited extra merits on high stability, facile separability, and long-term reusability. The reductive amination of furfural with other N-containing compounds (e.g., aminopropanol, glycine and β-alanine) also proceeded well depending on the type of heterogeneous catalysts, giving rise to 50-90 % yields of the corresponding target amines. Based on the above findings in relation to the reductive amination of furfural, it can be clearly induced that the current state of relevant works commonly has one or several of the following issues<sup>3, 4, 9, 11-14, 19-21</sup>: 1) noble metal-based homogeneous catalysts need complex or even toxic ligands, tedious product/catalyst separation process, difficult catalyst recycles and reusability; 2) heterogeneous catalysts with earth-abundant transition metal can induce reductive amination but

commonly requires harsh conditions; 3) structural features of heterogeneous support obviously affect the catalytic activity and selectivity, which requires a more simplified method in catalyst preparation. In attempt to overcome these problems, especially for the development perspectives with sustainable and environmental goals in the near future, several main factors are necessary in providing a relatively brand-new methodology of reductive amination, i.e., green and renewable reacting reagent, a full atom-economic process without any by-product generation, fairly cheap and possible widely applied industrial scalable heterogeneous catalysts, relatively mild condition, easy and convenient procedures of product separation and downstream processing.

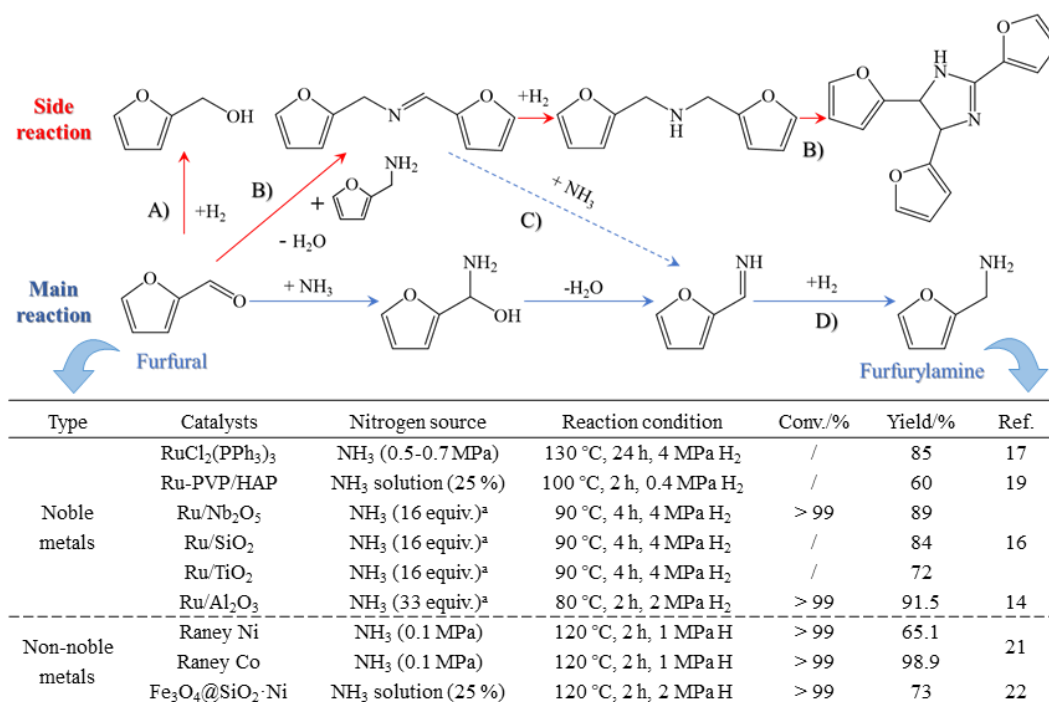


Fig.1 Reductive pathway for the reductive amination of furfural with ammonia and the summary of relevant studies. Note: <sup>a</sup> Molar equivalent relative to furfural; <sup>b</sup> conversion of furfural; <sup>c</sup> yield of furfurylamine.

Herein, we describe an environmentally friendly and simplified procedure for the preparation of porously graphitic spheres that encapsulate uniform cobalt nanoparticles (Co@C) by adopting cobalt acetate as the precursor. This strategy originates from the “chainmail for catalyst” provided by the group of Bao et al.<sup>23, 24</sup>, who have elaborated the unique electron penetration through the graphene layer from the encapsulated metals to promote relevant catalytic reaction on the outermost surface of graphene. We avoid the use of hazardous solvent and meanwhile reduce the number of synthetic steps as described in the experimental section. The structural features of catalysts in relation to its catalytic activity were characterized by multiple technique, and the selected catalysts were next applied to the challenging reductive amination of furfural for the synthesis of functional amines under varied conditions (70-120 °C, 1-5 MPa H<sub>2</sub>, and 1-5 h in this study) to investigate the effects of operational factors. Subsequently, using the optimized conditions and starting from inexpensive, readily available reactants and molecular ammonia, we conducted the synthesis of more than 24 biomass-derived platforms for a series of primary amines with varied functional groups. Last but not least, we have also demonstrated the scale-up of the heterogeneous amination protocol to gram-scale synthesis as well as

lifecycle performance in batch reactor to prove the value in industrial application, which can provide an available preparation of simple but highly efficient catalysts for the reductive amination of renewable sources in near future.

## 2. Experimental section

### 2.1 Chemical materials

The chemicals and solvents used in this study were purchased from the certified companies registered in China Academy Science On-line market systems, such as Aladdin Chemicals Co. Ltd. (Beijing, China), Sigma-Aldrich Chemicals Co. Ltd. (Shanghai, China), and Macklin Chemical Reagent Co., Ltd. (Shanghai, China). All of them were used without any preparation, but the purity of substrates was determined prior to experiments, such as furfural ( $\geq 98.5\%$ ), 5-HMF ( $\geq 99\%$ ), and furfurylamine ( $\geq 99\%$ ).

### 2.2 Preparation of the heterogeneous catalyst

The cobalt-based catalyst with porously graphitic structures was synthesized through a simplified three-step procedure described in our previous work<sup>25</sup>. Initially, citric acid (as carbon source, 0.03 mol) and cobalt acetate (as Co source, 0.03 mol) were assembled in H<sub>2</sub>O at approximate 70 °C to form an aqueous mixture, where the solvent was very slowly evaporated in a vacuum environment within 72 h so as to enable a well distribution of metallic atoms. The aqueous mixture could be coagulated like a sparking jelly if most of solvent was successfully escape from the mixture systems, serving as the carbonaceous precursor coated with cobalt acetate. It is noteworthy that since the choice of solvent and cobalt source affects heterogeneous catalyst properties to a large extent, so that less hazardous solvent (e.g. EtOH) and other cobalt salts (e.g., cobalt nitrate, cobalt carbonate) were also investigated as a reference; however, the preliminary results reflected that the influence of solvent was much important than that of cobalt salts. Afterwards, the carbonaceous precursor was pyrolyzed at 500-700 °C for 3 h under N<sub>2</sub> atmosphere in a constant flow of 40 ml/L, and then rinsed with the 1 M H<sub>2</sub>SO<sub>4</sub> and H<sub>2</sub>O to remove the unloaded metals and readjust the pH of catalyst back to 7, respectively. A cobalt encapsulated in graphene layer (Co@C) nanoparticles catalyst could be obtained after vacuum freeze-drying at -41 °C overnight. Some of Co@C catalyst were further oxidized under O<sub>2</sub>/Ar (5% O<sub>2</sub> in Ar, 99.999% purity) atmosphere at 200 °C for 3 h to provide the Co/CoO@C catalyst, which is helpful to distinguish the catalytic properties between metallic atoms and oxides. All of these materials were labeled as Co/CoO@C-*x*-*y*, where *x* suggests the pyrolysis temperature, and *y* denotes the solvent. These controllable factors associated with the preparation of cobalt-based catalyst were discussed in detail by its structural features as well as catalytic activity so as to establish the correlation between processing conditions and catalyst properties.

### 2.3 Analysis of Catalyst properties

Generally speaking, the performance of heterogeneous catalysts is commonly characterized by two

important aspects: one is relevant to the structural features of carbonaceous support, while another associated with the catalytic activity is closely related to the metallic nanoparticles. In attempt to explore the comprehensive information, both of them were analyzed with the help of multiple techniques as described below.

As for the structural features of carbonaceous support: 1) the morphological information was measured using a high resolution transmission electron microscopy (HRTEM), and another high-angle annular dark-field scanning transmission electron microscope (HAADF-STEM; JEM-2100F, Japan) was coupled with an energy dispersive X-ray spectrometry (EDS; Thermo Scientific, Waltham, MA) to measure the distribution of metallic atoms. At the same time, the surface appearance of sample was investigated by scanning electron microscopy (SEM, S-4800, HITACHI, Japan). The surface area and pore structure of samples were also analyzed through a Micromeritics Gemini VII 2390 gas-adsorption analyzer according to the N<sub>2</sub> isothermal adsorption/desorption at -186 °C in the relative pressure ( $P/P_0$ ) between 0.01 and 0.99; 2) the crystal structure was explored with the help of XRD (PANalytical, X'Pert PRO, Netherlands) by employing Cu K $\alpha$  radiation ( $\lambda=0.15406$  nm), and the scan conditions were adjusted from 20° to 80° in  $2\theta$  range with 0.0167° step interval. Additionally, given the correlation of Raman spectra with the parameters calculated from XRD, a Raman spectrometer (LabRAM HR800-LS55, France) was applied for the specific microstructure information of cobalt-based catalysts. The light source was provided by Nd-YAG at 532 nm, and the scanning region was selected between 1800 cm<sup>-1</sup> and 1000 cm<sup>-1</sup>. XPS analysis was adopted to characterize the surface chemistry, especially for cobalt and carbon functionalities, of solid samples to a depth of around 0.1–1 nm. XPS spectra were obtained on a Thermo Scientific ESCALAB 250Xi spectrometer, which equipped with Al (K $\alpha$ ) X-ray radiation source ( $h\nu=1486.6$  eV) at a 20 eV pass energy, a 0.1 eV energy step and 0.1 s dwelling time.

As for the catalytic activity of metallic nanoparticles: 1) the total acidity and acid strength distribution were determined by temperature-programmed desorption of ammonia (NH<sub>3</sub>-TPD) with an ASIQUACIV200-2 automatic physical/chemical adsorption analyzer (Quantachrome, U.S.). The sample (150 mg) was loaded into the U-tube quartz reactor and heated to 200 °C for 30 min (heating ramp of 10 °C/min) under 30 mL/min of He flow. The system was cooled to 80 °C, 8% NH<sub>3</sub>/He mixed gas was adsorbed onto the catalyst for 60 min until the saturation state was obtained and then the catalyst was purged with a He flow of 30 mL/min to remove the physically adsorbed NH<sub>3</sub>. Next, the system was heated to 525 °C with a heating ramp of 10 °C/min under the same He flow. H<sub>2</sub>-TPR were performed with the same scheduler, except the gas NH<sub>3</sub> was accordingly changed to H<sub>2</sub>; 2) distribution of Brønsted (B) and Lewis (L) acidity of the catalysts were examined by pyridine-adsorbed Fourier transform infrared spectrometer (Py-FTIR; Nicolet 6700, Orlando, FL). A 100 mg sample was vacuum-activated ( $1\times 10^{-4}$  mmHg) at 200 °C for 60 min. The background spectrum was recorded after sample cooling to 50 °C, then the sample was exposed to pyridine (Aldrich, GC, purity  $\geq 99.5$  %) vapor

for 15 min. Afterward, pyridine was performed vacuum-desorption at 40, 200, and 350 °C for 30 min; 3) *in-situ* FTIR absorption spectra were determined on a Nicolet iS50 FTIR spectrometer (Thermo Fisher, USA), whose resolution was set as 4 cm<sup>-1</sup> and the scan was executed 64 times. The prepared catalysts were pressed into a cell equipped to allow online sampling under 10% H<sub>2</sub>/He at 400 °C for 30 min, and were then cooled to 25 °C under vacuum environment. The backgrounds were collected at that situation, and the samples were subsequently exposed to 5% CO/He atmosphere at 25 °C for 60 min to record FTIR spectra.

#### 2.4 General procedure of the reductive amination

The reductive amination of furfural and other biomass-derived platforms were performed in a stainless steel autoclave reactor (MS100-P5-T3-HC1-SV, Anhui Kemi Machinery Technology Co., Ltd., China), coupled with six independent channel (each of them is 10 ml). In a typical run, 0.5 mmol furfural, 10 mg catalyst, and 5 ml 7 M NH<sub>3</sub> (in MeOH) were accurately weighted into one of the channel; subsequently, the reactor was flushed with H<sub>2</sub> for several times to remove air, and charged 2 MPa H<sub>2</sub> at the final time. The reactor was then heated up to the target temperature for a given period, and the magnetic stirrer was rotated at a constant speed of 30 rpm throughout the whole period to ensure the homogeneous reaction. Afterwards, the products in mixture was filtered and primarily detected by gas chromatography using 1,3,5-trimethoxybenzene as internal standard. The products were also identified by GC/MS (Thermo Trace 1300-ISQ QD, USA) and <sup>1</sup>H NMR (Avance III 400MHz NMR, Bruker, Germany) to calculate the corresponding conversion and selectivity. Further studies on the influence of reaction conditions includes the temperature range of 60-120 °C, the reaction time of 0-8 h, the catalyst amount of 5-15 mg, the NH<sub>3</sub> aqueous concentration of 2-7 M, and the H<sub>2</sub> pressure of 1-5 MPa. Scope of substrates limits on the typical biomass-derived platforms, involving 5-HMF, substituted furfural, or phenol derivatives.

### 3. Results and discussion

#### 3.1 Structural and catalytic features of catalyst

First of all, the SEM were taken to primarily investigate the morphological structure of catalysts. As shown in Fig.2 (a)-(c), the magnified images exhibit that the anomalous sponge-like structure were observed for these catalysts, and this trend was more serious with the increasing pyrolysis temperatures because that of Co@C-700-EtOH started to collapse into smaller particles with large pores. Such sponge-like structures were mainly caused by the volatilization of organic matter during the pyrolysis stage to form a heterogeneous material<sup>26</sup>, which could assemble the metallic nanoparticles depending on its pore size, as reported by Lu et al.<sup>27</sup> in their studies. Interestingly, an extra step of oxidation at 200 °C for 3 h might result in the formation of crystal cubes or rods as part of metallic nanoparticles were aggregated/oxidized into a relatively large size (displayed at Fig.2 (e)). The corresponding EDS of Co/CoO@C-600-EtOH result reveal the coexistence of C, O, Co with a

mass fraction of 76.3 %, 18.0 % and 5.7 %, respectively, where the ratio of C and O was superior to that of Co@C-600-EtOH owing to the superficial oxidation of cobalt nanoparticles in air, coinciding with the similar observations on crystal structures reported previously<sup>18, 28</sup>.

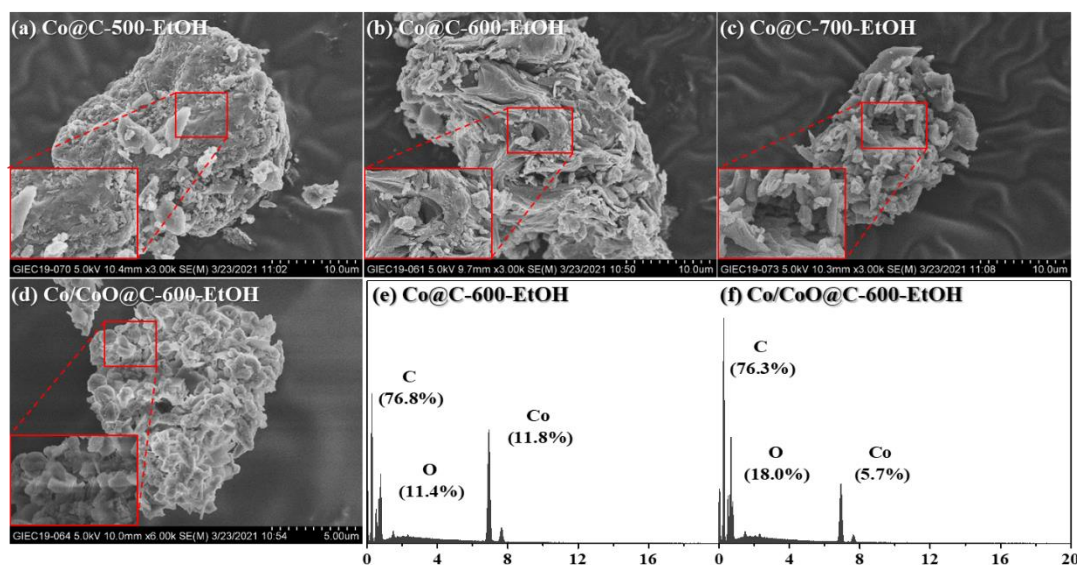


Fig.2 SEM image of Co@C-500-EtOH (a), Co@C-600-EtOH (b), Co@C-700-EtOH (c), and Co/CoO@C-600-EtOH (d), together with the corresponding EDS results of Co@C-600-EtOH (e) and Co/CoO@C-600-EtOH (f).

In addition, the prepared catalysts were subsequently analyzed using TEM to observed the distribution of supported metal on nanoparticle surface and its average size as shown in Fig.3 (a) and (b). It is obvious that the metallic nanoparticles were dispersed uniformly on the surface of carbonaceous matrix and completely coated by graphene shells without any significant aggregation of clusters. Use of ethanol instead of H<sub>2</sub>O as solvent made it gradually coated on individual metallic nanoparticles. According to the statistical data, we can found that the average diameters of these metallic nanoparticles were  $5.56 \pm 0.35$  nm (Co@C-500-EtOH),  $6.82 \pm 0.42$  nm (Co@C-600-EtOH),  $7.31 \pm 0.28$  nm (Co@C-700-EtOH), and  $8.32 \pm 0.24$  nm (Co/CoO@C-600-EtOH), indicating that 1) at temperature over 500 °C, the metallic nanoparticles were finally obtained by encapsulation of graphene layers on the surface, and the layer number could be controlled by the pyrolysis temperature<sup>29</sup>; 2) the extra step of oxidation could promote the growth and agglomeration of cobalt oxides, thus causing the poor dispersity<sup>30</sup>. A well-resolved fringes with an interplanar spacing of 0.20 nm can also be clearly observed in Co@C-600-EtOH, which is attributed to the (111) plane d-spacing of the Co metal (i.e., Co<sup>0</sup>) in the Co@C-600-EtOH. In view of these results, it can be proposed that Co<sup>2+</sup> in the structure of carbonaceous precursor was reduced during the pyrolysis process to Co<sup>0</sup>, and that the final size of the formed Co nanoparticles can be controlled by varying the pyrolysis temperature<sup>28</sup>. By contrast, the metallic nanoparticles in the Co/CoO@C-600-EtOH samples not only had the (111) plane of the Co metal, but also exhibited the (111) plane of the CoO alloy with a d-spacing of approximate 0.25 nm<sup>31</sup>. These crystal plane exactly agrees with the number of diaphragm shown in their corresponding diffraction pattern, which were

discussed together with Raman spectra in the following section. Moreover, the corresponding elemental mappings given in Fig.3 (c)-(f) also suggested the homogeneous distribution of Co atoms over the particle surface of Co@C-600-EtOH, whereas that of Co/CoO@C-600-EtOH suggested a higher concentration of oxygen species which are well coexisted with Co atoms as cobalt oxide (CoO), in good agreement with the result of TEM images. By and large, most of these metallic atoms are surrounded by a combination of some graphitic layers and short-range ordered graphitic shells, functioning as chainmail for catalyst which are accessible to reactants and performed as active center for catalytic reaction.

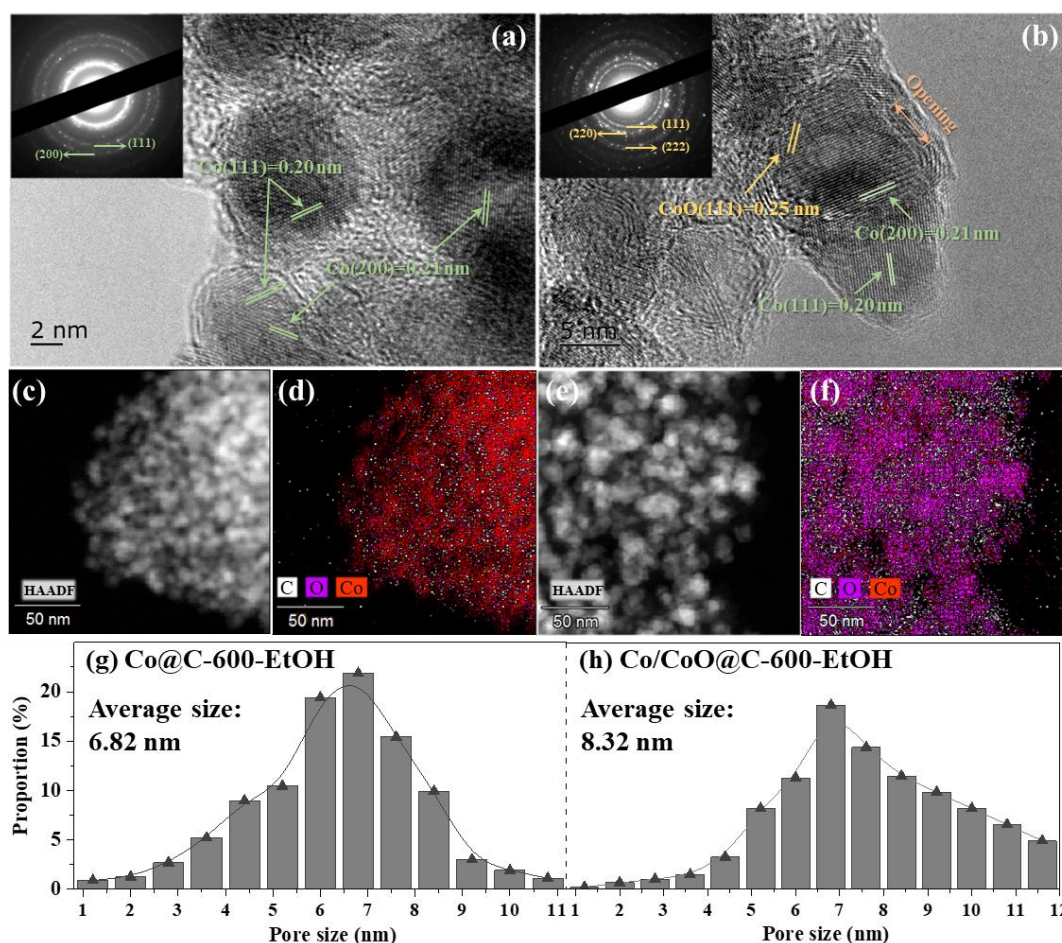


Fig.3 TEM image of Co@C-600-EtOH (a) and Co/CoO@C-600-EtOH (b), and insets in here show the corresponding diffraction pattern; HAADF-TEM images of single particle in Co@C-600-EtOH (c) and Co/CoO@C-600-EtOH (e) with their elemental mapping of C, O, and Co in (d) and (f), respectively; the statistical results of the size distribution for Co@C-600-EtOH (g) and Co/CoO@C-600-EtOH (h).

The N<sub>2</sub> adsorption-desorption isotherms of the prepared catalyst at 77 K were adopted to analyze the specific surface area through the Brunauer-Emmett-Teller (BET) method, while the pore structure was calculated using the Barrett-Joyner-Halenda (BJH) model to identify the proportion of microporous to mesoporous distribution (0.35-40 nm)<sup>28, 31, 32</sup>. As shown in Fig.4 (a), all of the prepared catalysts presented a typical type of IV (i.e., Langmuir adsorption-desorption isotherms), corresponding to a well-developed micro- and mesoporous structure, as a large amount of N<sub>2</sub> was mainly adsorbed in the entire relative pressure range<sup>32</sup>. In here, the hysteresis loop suggested that a capillary condensation was occurred at desorption stage and led to the lower

$P/P_0$  than that at adsorption process with the same quantity<sup>28</sup>. With the increasing pyrolysis temperature, it can be observed that the specific surface area of catalyst was gradually increased from 297.4 m<sup>2</sup>/g (at 500 °C) to 407.8 m<sup>2</sup>/g (at 600 °C) due to the devolatilization process where the organic matter was escaped in the forms of CO<sub>2</sub>, leading to the opening of pore structure confirmed by SEM images; however, another slight decrease was detected for Co@C-700-EtOH (375.2 m<sup>2</sup>/g) because of the collapse of pore at severe conditions. Additionally, Co/CoO@C-600-EtOH catalyst prepared with an extra oxidation step had the similar but relative lower specific area than that of Co@C-600-EtOH, which implied the introduction of oxygen would assemble more metallic oxides thereby slightly blocking pore structure. More importantly, such hierarchical porosity of the Co@C is of great important for the catalysis application, as the heterogeneous porous property could facilitate the chemisorption and dispersion of metal particles according to relevant literature<sup>31</sup>. It was also noted in Fig.4 (b) that all of samples displayed a peak centered at around 6.5 nm, indicating that the heterogeneous materials are dominated by a mesoporous structure that can enhance catalytic activity and provide efficient diffusion<sup>33</sup>. The average pore diameters of the Co@C-600-EtOH and Co/CoO@C-600-EtOH are calculated to be 5.6 and 4.9 nm, while the corresponding total pore volumes are 0.801 and 0.687 cm<sup>3</sup>/g, respectively. Interestingly, some early studies demonstrated that catalyst containing large pores could lead to the rapid transportation of products and reactants, thus influencing selectivity for reduction amination<sup>32, 33</sup>.

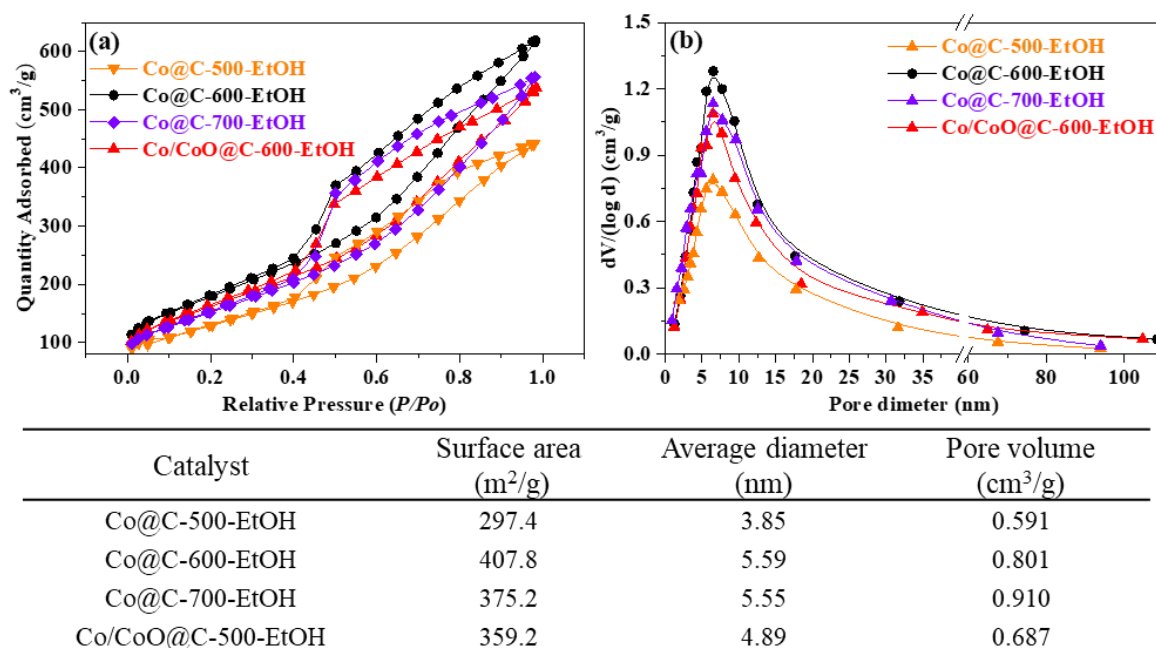


Fig.4 N<sub>2</sub> adsorption-desorption isotherms and pore size distribution of the prepared catalysts

To further investigate the structure-activity relationship, several techniques including XRD, Raman, FTIR, and XPS were adopted for a comprehensive understanding, whose results were provided in Fig.5. From the XRD patterns depicted in Fig.5 (a), it can be found that only three characteristic peaks corresponding to the planes of Co metal (i.e., 43° (111), 52° (200), and 75° (220)) were observed in Co@C-600-EtOH when compared to Co/CoO@C-600-EtOH, and all of them are relatively narrow and sharp in metallic states which

indicated that the Co@C-600-EtOH sample have high purity levels, single crystal phases, and high structural regularities<sup>28, 34</sup>. After being oxidized under 5% O<sub>2</sub>/N<sub>2</sub> atmosphere at 200 °C, the reflected planes of Co metal have been weakened or even eliminated, but following with the newly developed peaks at 37° (111), 65° (220) and 78° (222) that could be ascribed to the incorporation of O into the lattice of cobalt metal to form cobalt oxides<sup>31</sup>. The broad reflection of Co/CoO@C-600-EtOH implied an amorphous structure which might limit the active sites, affecting the catalytic activity during reduction amination<sup>35, 36</sup>. This can also be inferred from the Raman spectra shown in Fig.5 (b), where the spectra of heterogeneous materials exhibited a D band at around 1350 cm<sup>-1</sup> and a G band at around 1580 cm<sup>-1</sup>, corresponding to the disordered arrangement of graphite lattice structures and the stretching of *sp*<sup>2</sup> atomic pairs on carbon ring or long carbon-chain in graphite, respectively<sup>36</sup>. The value of *I*<sub>D</sub>/*I*<sub>G</sub> was calculated through the strength of D and G bands as previously reported (Co@C-600-EtOH: 27.5; Co/CoO@C-600-EtOH: 23.0), which confirmed that the oxidation step reduced the graphitization of carbon-supported catalysts<sup>37</sup>. Acid functional groups were detected on the catalyst surface by means of FTIR spectra shown in Fig.5 (c), where the wide peak of ν-O-H (between 3600 cm<sup>-1</sup> and 3200 cm<sup>-1</sup>) and the peak of ν-C-O (between 1100 cm<sup>-1</sup> and 1000 cm<sup>-1</sup>) were attributed to the hydroxyl group, while the peak of ν-C=O (between 1760 cm<sup>-1</sup> and 1680 cm<sup>-1</sup>), ν-C-O (between 1320 cm<sup>-1</sup> and 1210 cm<sup>-1</sup>) and δ-O-H (between 955 cm<sup>-1</sup> and 915 cm<sup>-1</sup>) reflected the existence of carboxyl group<sup>35</sup>. Both of the prepared catalysts exhibited the sufficient amount of acid sites which can probably catalyze the reductive amination. In addition, the characteristic peaks associated with aromatic structures (ν-C=C and ν-C-C) were found to be strong in the range of 1650 cm<sup>-1</sup> to 1450 cm<sup>-1</sup>. The chemical states and the surface properties of metal functions were also studied by XPS spectra to understand the interaction between carbon and cobalt species, as shown in Fig.5 (d)-(e). In the C 1s spectra, the wide peak ranging from 282 eV to 295 eV can be resolved into individual peaks at approximate 283.9 eV, 284.8 eV, 286.2 eV, 287.6 eV, and 289.1 eV, which were in accordance with the -C-H bonds, the -C-(C, H)/C=C bonds in graphitic structures, -C-(O, N) graphene bonds, -C=O bonds, and O-C=O bonds, respectively<sup>26, 30, 36</sup>; among them, the bond of -C-(C, H)/C=C was dominant but suffered from a slight decrease after oxidation. Further, it is also noted that the chemical state of Co 2*p* was mainly in metallic form with the binding energy of Co 2*p*<sub>3/2</sub> spectrum at around 778 eV, while that of Co 2*p*<sub>1/2</sub> belonged to the oxidized form of Co<sup>2+</sup> located at 789 eV<sup>28, 30</sup>. A strong Co 2*p*<sub>3/2</sub> satellite peak at 786 eV and Co 2*p*<sub>1/2</sub> satellite peak at 796 eV were found, which has been used for the identification of cobalt species<sup>31</sup>. The varied intensities of specific peaks for different catalyst were in well agreement with this trends, such as the oxidation step strengthened the peak of Co 2*p*<sub>1/2</sub> as well as weakened that of Co 2*p*<sub>3/2</sub>, which drew a conclusion that the functions of Co<sup>0</sup> and Co<sup>2</sup> in the catalysts might be affected by the preparation condition in a mutual way.

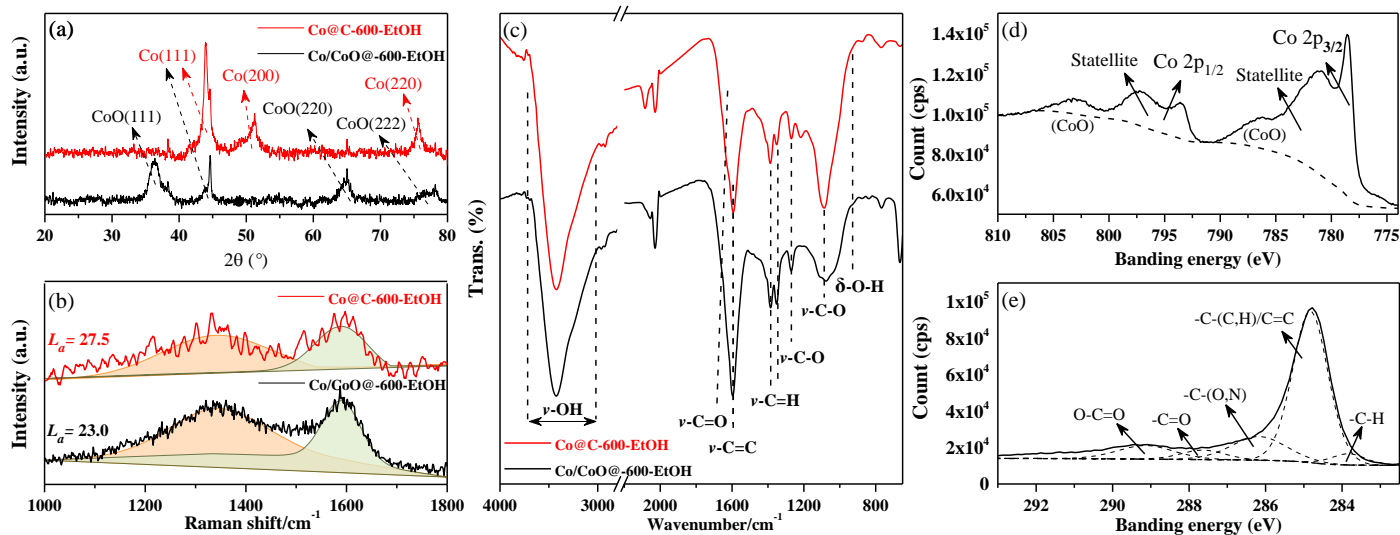


Fig.5 Structural features of the prepared catalyst. XRD results of Co@C-600-EtOH and Co/CoO@C-600-EtOH (a); Raman spectra of Co@C-600-EtOH and Co/CoO@C-600-EtOH (b); FTIR spectra of Co@C-600-EtOH and Co/CoO@C-600-EtOH (c); XPS image of Co@C-600-EtOH related with its spectrum (d) and Co spectrum (e).

In attempt to identified the effect of acidity on catalytic activity, the relevant types and total amount of acid sites were collaboratively examined by NH<sub>3</sub>-TPD and Pyridine-IR adsorption, whose profiles were depicted in supplementary information. The NH<sub>3</sub> desorption peaks positioned at the temperature of 200 °C were clearly observed for both of Co@C-600-EtOH and Co/CoO@C-600-EtOH, and this might be assigned to the acid sites of the hydroxyl groups on particle surface<sup>31</sup>. At higher temperature, two strong desorption peaks at around 273 °C and 488 °C were observed for Co@C-600-EtOH, suggesting the existence of strong acidity. However, it is found that NH<sub>3</sub> desorption peaks of Co/CoO@C-600-EtOH was relatively small, which indicated that the amount of strong acid sites was few. As for the type of acid sites, the Py-IR spectroscopy were further detected at around 1650 cm<sup>-1</sup> and 1400 cm<sup>-1</sup>, where the reflection bonds at 1450 cm<sup>-1</sup> and 1600 cm<sup>-1</sup> were all ascribed to the Lewis acid sites, meanwhile an obvious reflection of the Brönsted acid site was also observed at 1540 cm<sup>-138</sup>. In general, the Brönsted acid sites could be attributed to the hydroxyl groups on the particles and easily to be dissociated at high temperature. While, the introduced Co species can act as Lewis acid sites or electrophilic sites to polarize and facilitate the cleavage of C-O bond<sup>37</sup>. Besides, the active sites of metallic nanoparticle were determined by the H<sub>2</sub>-TPR as its peak position could be inferred to the reduction difficulty, and the results of H<sub>2</sub> consumption under different situation were also provided in supplementary information. Noticeably, there was a well-defined reduction peak evolving at above 500 °C for Co/CoO@C-600-EtOH, which was ascribed to the Co<sup>2+</sup> species reduction. On the other hand, no evidence of this reduction was seen in the Co@C-600-EtOH sample but with an obvious degree of reduction at lower temperature, suggesting more active sites of metals were observed.

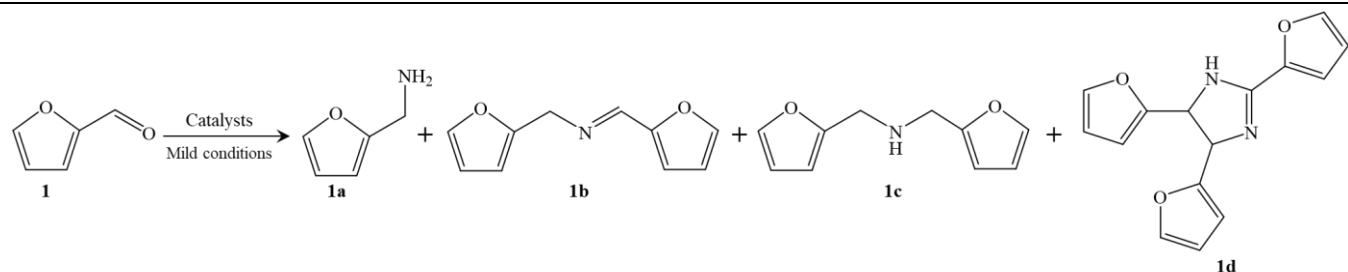
## 3.2 Catalyst application on the reaction of reductive amination

### 3.2.1 Catalyst screen for the reductive amination of furfural

The catalytic activity and selectivity of a series of catalysts was evaluated by the reductive amination of furfural in the presence ammonia solution and H<sub>2</sub> to produce the target product (i.e., furfurylamine), which was presented as a structural motif in several bioactive molecules. Some of the commercial catalysts including 5% Ru/C, 5% Pt/C, 5% Rh/C, 5% Pd/C, Raney Co and Raney Ni were also considered for comparison in this experiments. In terms of the target product described at Table 1, it could be found that the change of pyrolysis temperatures in the preparation of catalysts strongly affects its catalytic selectivity for 1a in the reduction amination of furfural (Entry 1-3), suggesting that an ideal temperature of 600 °C is recommended. The use of EtOH could also improve the catalytic selectivity for 1a when compared to the catalysts prepared in H<sub>2</sub>O (Entry 2, 4). Several sources of cobalt compounds involving cobalt acetate, cobalt carbonate, and cobalt nitrate indicated similar effects on the catalytic activity and selectivity. However, the introduction of oxygen atoms during oxidation step significantly decreased the catalytic selectivity for 1a (Entry 5). It can be concluded that the best catalyst according to our experimental procedure is Co@C-600-EtOH, whose catalytic activity and selectivity to yield 1a reach more than 99 % and 86 %, respectively. By contrast, most of noble-based catalysts (i.e., 5 % Ru/C, 5 % Pt/C, 5 % Pt/C, and 5 % Pd/C) exhibited a lower selectivity for reductive amination (Entry 6-9), and the use of commercial Raney Co afforded a yield of 83.7 % for 1a while Raney Ni only yield 64.8 % (Entry 10,11).

Form these results, the reductive amination can be successfully done by using the Co@C-600-EtOH sample under very mild reaction conditions, but several side reactions were one of the main reason for the carbon loss according to the reaction formula of reductive amination illustrated in Table 1. In addition to furfurylamine, another condensation product of N-furfurylidenefurfurylamine (i.e., 1b) was identified to be one of the intermediates for the reductive amination of furfural. The hydrogenation of N-furfurylidenefurfurylamine could easily produce the by-product of Difurfurylamine (i.e., 1c), while its subsequent thermal cyclization to furfural (i.e., 1d) has also been noted in previous works<sup>39</sup>. Interestingly, the hydrogenation of furfural into furfuryl alcohol was not detected in our catalyst system, which was commonly observed in other catalytic systems, especially using noble metal catalyst<sup>6</sup>. This might be caused by the fact that the cobalt-based catalysts were inactive towards the hydrogenation of furfuryl alcohol, in accordance with the higher selectivity towards furfurylamine in Raney Co system when compared to that of Raney Ni (Entry 10,11). Xu et al.<sup>21</sup> also confirmed that the cobalt nanoparticles were identified as the active sites for the reductive amination, which is very meaningful to get a satisfied yield of target product.

Table 1 Reductive amination of furfural over different catalysts



Entry	Catalysts	Conv. / %	Yield of <b>1a</b> / %	Entry	Catalyst	Conv. / %	Yield of <b>1a</b> / %
1	Co@C-500-EtOH	> 99	80.4	6	5 % Ru/C	> 99	0.0
2	Co@C-600-EtOH	> 99	86.9	7	5 % Pt/C	> 99	81.1
3	Co@C-700-EtOH	> 99	71.5	8	5 % Rh/C	> 99	68.5
4	Co@C-600-H <sub>2</sub> O	> 99	47.2	9	5 % Pd/C	> 99	14.7
5	Co/CoO@C-600-EtOH	> 99	8.5	10	Raney Co	> 99	83.7
/	/	/	/	11	Raney Ni	> 99	67.8

Note: Screening of prepared and commercial catalysts are based on the below conditions: 90 °C, 2 h, 10 mg catalyst, 5 ml ammonia solution (7M NH<sub>3</sub> in MeOH), 2 MPa H<sub>2</sub>, and 0.5 mmol furfural; the better catalyst of Co@C-600-EtOH was selected to further optimize the reaction conditions. Yields and conversion were determined by GC-MS and <sup>1</sup>H NMR spectroscopy using 1,3,5-trimethoxybenzenen as an internal standard.

### 3.2.2 Optimization of the reaction conditions for the reductive amination of furfural

In order to get the highest yield of target products, the reaction conditions have to be optimized. Firstly, the effect of reaction temperature on the reductive amination of furfural was studied under 2 MPa H<sub>2</sub> pressure in the presence of 5 ml of 7M NH<sub>3</sub> solution (in MeOH), and the variation of several products were depicted in Fig.7 (a). As can be seen, furfural could be completely converted even at 60 °C, but the catalytic selectivity towards furfurylamine remained at a very low level of 3.4 %. The yield of furfurylamine was found to have a positive relationship with reaction temperature, increasing up to 92.4 % with the elevation of temperature from 60 °C to 120 °C; however, the most obvious increase occurred between the range of 60-90 °C where the yield of furfurylamine could reach a relatively high level of 85.8 %. Difurfurylamine were observed at first but nearly not produced at higher temperature, which suggested that the transformation of N-furfurylidene-furfurylamine into furfurylamine was promoted by the reaction temperature, while the side reaction of the hydrogenation of intermediates into Difurfurylamine was thus inhibited<sup>39</sup>. The formation of furfural caused by the thermal cyclization always existed but with a negligible value less than 2.8 %. Considering the catalytic selectivity as well as the economic benefits of reaction conditions, the reaction temperature at 90 °C was selected for the subsequent experiments.

With the optimal reaction temperature in hand, the time course of the products distributions was recorded for the reductive amination of furfural with NH<sub>3</sub> and H<sub>2</sub> as shown in Fig.6 (b). For all cases, the conversions of furfural were high to quantitative (high than 99.5 %); as far as the target product, the molar percentage of furfurylamine greatly increased from 2.1 % at zero hour to 44.3 % at 1 h, 78.8 % at 2 h and 86.2 % at 4 h,

following with a constant level even prolonging reaction period up to 8 h. The variation of by-products through side reactions were also observed and suffered from a similar tendency with that of temperatures<sup>32</sup>. With regard to the influence of catalyst addition (shown in Fig.6 (c)), the use of 5 mg was sufficient to fully convert furfural but only yield 10.2 % furfurylamine, and this might be owing to the fact that a large number of furfural tended to react with the produced furfurylamine for N-furfurylidene-furfurylamine without the help of Co@C-600-EtOH catalyst. Accordingly, adding more catalyst could improve the catalytic selectivity for target products up to 87.6 %. It was also noted that the use of 10 mg was the threshold value as the further increase of catalyst gave limited effects on catalytic selectivity. Moreover, effects of NH<sub>3</sub> concentration on the reductive amination of furfural was also illustrated in Fig.6 (d). In contrast to the aforementioned factors, the NH<sub>3</sub> concentration exhibited a relatively weaker effects on the distribution of products, and the yield of furfurylamine could be accumulated with the increasing concentration of NH<sub>3</sub> to some extent. For example, the selectivity of furfural into furfurylamine was calculated to be 76.9 % by the use of 2M concentration of NH<sub>3</sub> in MeOH, while those were 83.3 % and 86.2 % in the presence of NH<sub>3</sub> solution of 5M and 7M, respectively. Last but not least, the H<sub>2</sub> pressure also reflected a slight effect on the conversion of furfural and its selectivity towards the target product, as shown in Fig.6 (e). All cases with the varied H<sub>2</sub> pressure between 1-5 MPa could provide the full conversion and the high selectivity of furfurylamine over 85 %. The by-product of Difurfurylamine was not observed under 1-2 MPa H<sub>2</sub> pressure, but it was produced under 3-5 MPa H<sub>2</sub> pressure with an increasing trend, whose selectivity was determined to be 3.4 %, 5.0 %, and 4.2 % under the H<sub>2</sub> pressure of 3, 4, and 5 MPa, respectively. This results suggested that both of the transformation of furfural into furfurylamine as well as the side product of Difurfurylamine were simultaneously promoted by the increase of H<sub>2</sub> pressures. Consequently, the optimal H<sub>2</sub> pressure of 2 MPa was adopted for the reductive amination of furfural, which provide not only the high conversion but also the high selectivity of furfurylamine.

During the process of reductive amination, N-furfurylidene-furfurylamine was identified to be the sole intermediate by gas chromatography, which was formed from the condensation of furfural with furfurylamine via the direct pathway according to the previous literatures<sup>13, 39</sup>; in here, methylfurimidate formed by the condensation of furfural with NH<sub>3</sub> was unstable to be detected by gas chromatography. The molar percentage content of Difurfurylamine was mostly eliminated after 4 h while the formation of furfurylamine kept almost unchanged, which suggests that the transformation of N-furfurylidene-furfurylamine into furfurylamine might be the rate determining step<sup>14</sup>. The addition of one NH<sub>3</sub> molecule to N-furfurylidene-furfurylamine gave rise to the instable germinal diamine, which was subsequently hydrogenated into furfurylamine. This was confirmed by the increased selectivity of furfurylamine by adding more NH<sub>3</sub> into the reaction systems discussed above. In summary, the reaction condition of 90 °C, 4 h, 2 MPa H<sub>2</sub>, 10 mg catalyst, and 7M NH<sub>3</sub> solution has been considered as the optimal conditions.

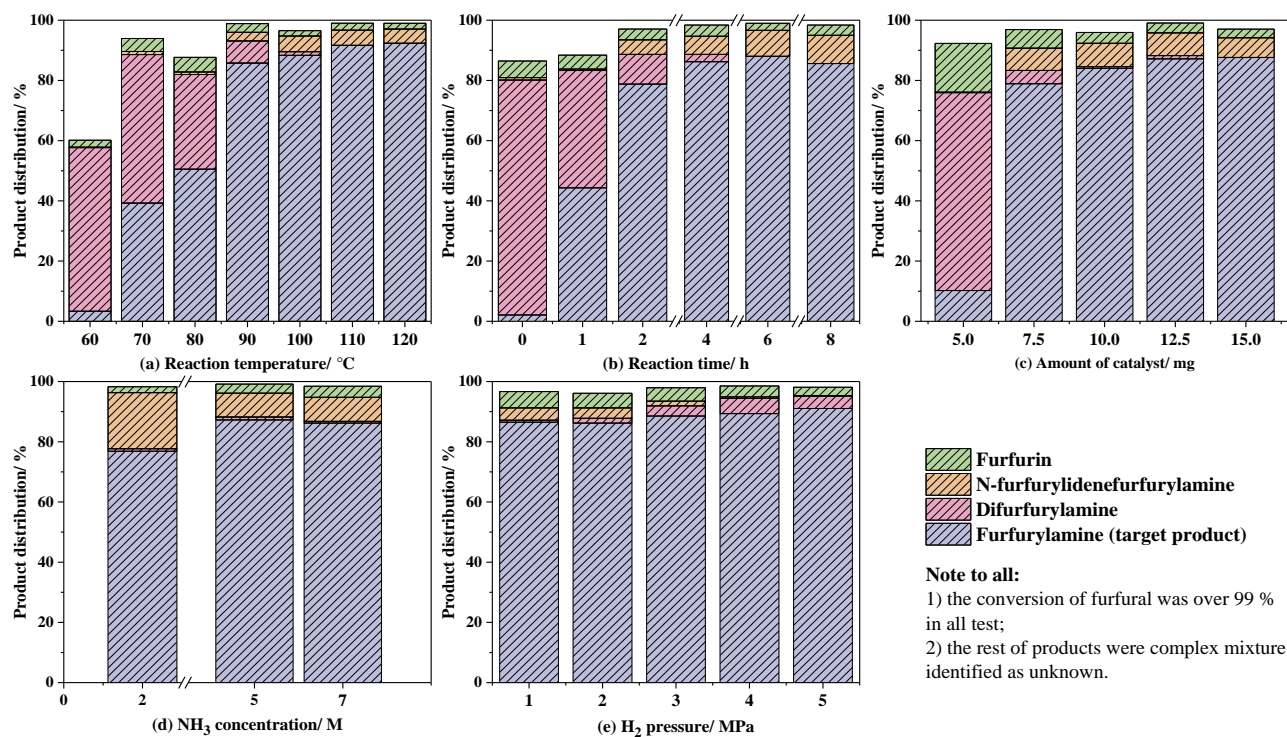


Fig.6 Influences of reaction conditions on the reductive amination of furfural. Reaction temperature (Entry 12-18), reaction time (Entry 19-24), amount of catalyst (Entry 25-29),  $\text{NH}_3$  concentration (Entry 30-33), and  $\text{H}_2$  pressure (Entry 34-38). Yields and conversion were determined by GC-MS and  $^1\text{H}$  NMR spectroscopy using 1,3,5-trimethoxybenzenen as an internal standard.

### 3.2.3 Substrate scope and the reaction mechanism

After selecting the suitable catalyst and the optimized reaction conditions from benchmark reaction, we next explored the substrate scope of catalyst in converting a wide range of biomass-derived platforms for the synthesis of primary amines via reductive amination, which can easily be functionalized further and thus serve as central building blocks for fine chemicals or pharmaceutical drugs<sup>6</sup>. As can be seen from Fig.7, the typical substrates derived from semi-/cellulose or lignin containing electron-withdrawing or electron-donating groups could be fully converted, affording the corresponding primary amines with good to excellent yield (Entry 39-57, 59, 61), except for vanillin and some phenol derives (Entry 58, 60). Among them, cellulosic biomass-derived HMF is another and renewable platform molecule, which represents a starting material to obtain sustainable access to various fine chemicals. Analogous to furfural, reductive amination of HMF constitutes a significant fundamental route for the sustainable production of N-containing compounds from renewable biomass. Some of the reported literatures also suggested that the reactivity of HMF in the reductive amination with gaseous or aqueous ammonia was superior to furfural in terms of target yield and reaction conditions<sup>21, 22, 40</sup>, in according with our results in Entry 39 and 41. Other kinds of biomass-derived platforms such as phenolic model monomers (e.g., phenol and substituted phenol) derived from lignin were also tolerated in our experiments (Entry 46-61). The substituted groups have no or slight effect on the catalytic activity/selectivity towards substituted compounds. Interestingly, no dehalogenation was observed in our catalytic system, which have been observed by other catalysts, especially noble metal catalysts<sup>41, 42</sup>.

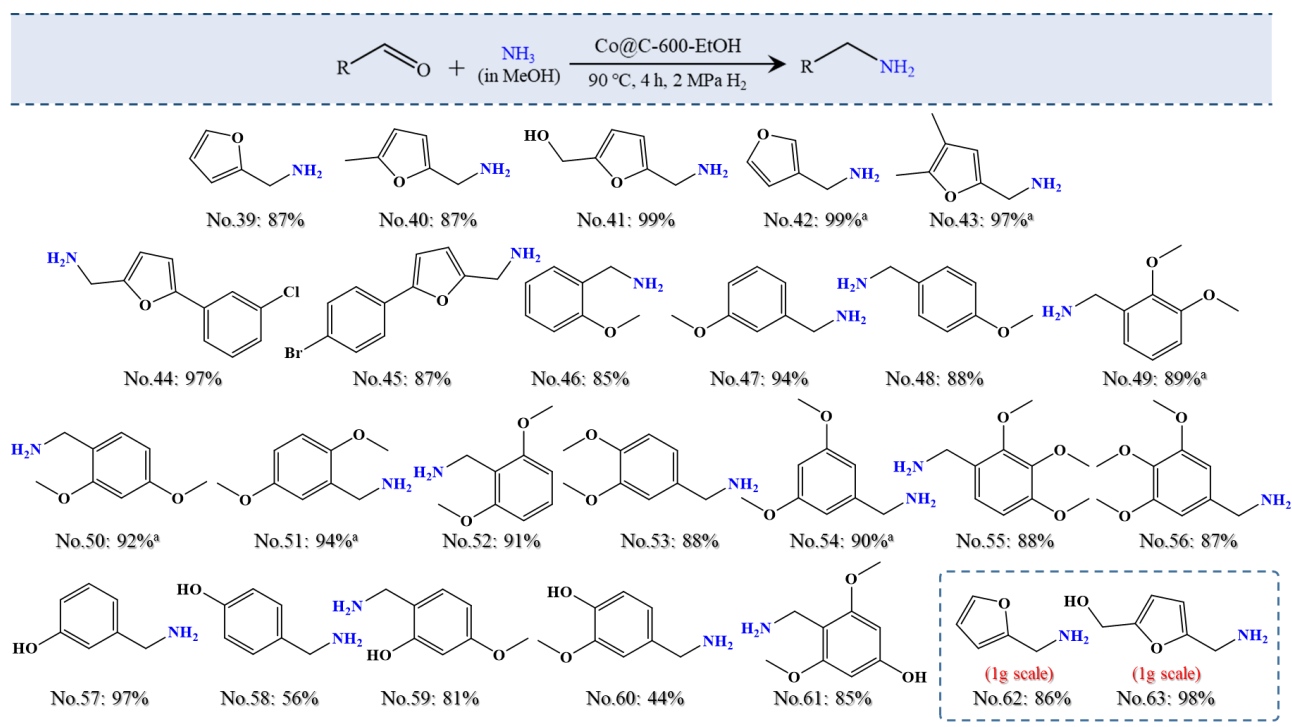


Fig.7 The result of reductive amination in terms of biomass-derived platforms for the synthesis of primary amines. Reaction conditions: furfural (0.05 mmol), 90 °C, 4 h reaction time, 10 mg catalyst, 7M NH<sub>3</sub> solution, and 2 MPa H<sub>2</sub> pressure. <sup>a</sup> Temperature was increased to 100 °C. Yields and conversion were determined by GC-MS and <sup>1</sup>H NMR spectroscopy using 1,3,5-trimethoxybenzenen as an internal standard.

According to our studies and controlled experiments, we proposed the mechanism of Co@C-600-EtOH on catalyzing the reductive amination of biomass-derived platform with NH<sub>3</sub> solution as N source. In this reaction process depicted in Fig.8, the furfural reacted with NH<sub>3</sub> first to form the intermediate methanol adsorbed on the catalyst surface, whose outer graphitic shell is activated by the electronic interaction between the inner metallic nanoparticles and the carbon layer as well as the induced charge redistribution<sup>23, 24</sup>. This characteristic facilitated the delivery of electron catalyzed by metallic cobalt, thereby forming imines after a dehydration reaction. In the following step, the H-H bond is activated on the surface of Co@C-600-EtOH, and in the meantime, the imine was reduced to furfurylamine by the introduction of H<sup>+</sup> under a very mild environment eventually<sup>39</sup>. The most accepted reductive amination pathway refers to the nucleophilic addition of amine and carbonyl groups to yield an imine, and the imine was then hydrogenated to the desired amine<sup>25</sup>. However, as for the second amines, the corresponding imine cannot be formed according to the above pathway. An *in-situ* Raman experiment was used to record the presence of intermediate species during the reaction under 80°C, whose results illustrated that the metallic Co promoted the imine formation by the activating C=O group of the aldehyde groups rather than the interaction between furfural and furfurylamine, while the acid sites on the particle surface was responsible for the hydrogenation of primary imines to the corresponding amines<sup>43</sup>.

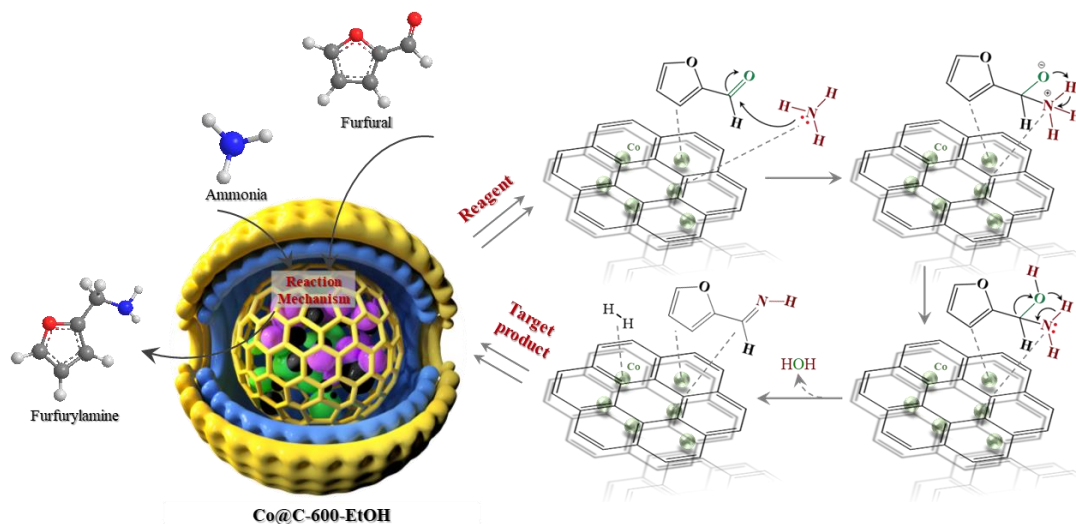


Fig.8 A possible pathway for the Co@C-600-EtOH catalyzed reduction amination of furfural with ammonia and H<sub>2</sub>

### 3.2.4 Lifecycle test

From the viewpoints of green chemistry, it is important to evaluate the stability and recyclability of catalysts as it represents the most essential characteristics for any industrial catalysts<sup>25</sup>. Apart from the apparent cost advantages associated with these characteristics and the ease of accessibility, the use of easily recyclable heterogeneous catalysts would remarkably support in product purification. For this reason, we evaluated the catalyst stability and recyclability on reductive amination of furfural at the end of this manuscript, mainly through the benchmark reaction under the suitable catalyst (i.e., Co@C-600-EtOH) and optimized reaction conditions (90 °C, 4 h, and 2 MPa H<sub>2</sub>) shown in Fig. 9. Surprisingly, in contrast to other commercial or previously reported catalysts, our graphene-shelled metallic nanoparticles exhibits great stability, which might be due to the fact that cobalt nanoparticles were embedded in the carbon layer as an armor so as to effectively protect leaching<sup>23</sup>. This catalyst could be immobilized on a magnetic stirring bar and be conveniently recycled up to eight times, but still having high product selectivity and catalyst activity. Furthermore, the catalyst without the acid-washing pretreatment was also adopted for the recycle test. The catalytic activity and selectivity for Co@C-600-EtOH without acid-washing pretreatment underwent a decrease at first and then followed the similar level with that of Co@C-600-EtOH having acid washing, which suggested that the exposed cobalt nanoparticles would be leached after several runs of test, but the cobalt nanoparticle embedded by carbonaceous graphitic structures work stable and sustainable.

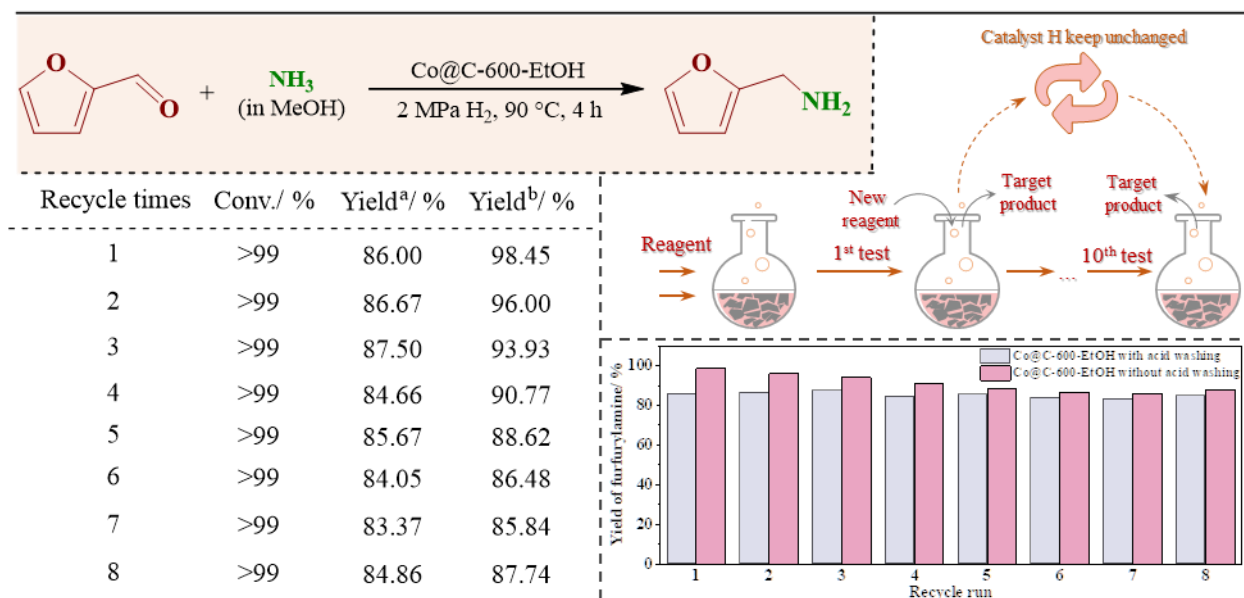


Fig.9 The recycling experiment of the Co@C-600-EtOH catalyst towards the reductive amination of furfural. Reaction conditions: furfural (0.05 mmol), 90 °C h reaction time, 4 h reaction time, 10 mg catalyst, 7M NH<sub>3</sub> solution, and 2 MPa H<sub>2</sub> pressure. Yield<sup>a</sup> and Yield<sup>b</sup> were calculated based on Co@C-600-EtOH with and without acid washing, respectively.

## 4. Conclusions

In summary, uniform nanoparticle catalysts encapsulated in multi-layer graphene structure using cobalt acetate as the precursor are synthesized successfully following with a simple and environmentally friendly method. According to its structural features associated with the catalytic activity and selectivity, we found that the metallic nanoparticles were dispersed uniformly on the surface of carbonaceous matrix and completely coated by graphene shells without any significant aggregation of clusters, and the sponge-like structures of heterogeneous materials was the reason for well distribution of metallic nanoparticles depending on its pore size. Besides, the introduced Co species can act as Lewis acid sites or electrophilic sites to polarize and facilitate the reductive amination, but an extra step of oxidation might significantly its catalytic selectivity. Influences of the processing conditions (i.e., temperature, time, H<sub>2</sub> pressure, NH<sub>3</sub> concentration, and amount of catalyst) affects the products distribution of reductive amination, and the optimized condition of 90 °C, 4 h, 2 MPa H<sub>2</sub> pressure, 7 M NH<sub>3</sub> solution, and 10 mg catalyst was applied. More importantly, under this mild industrially viable and scalable conditions, the catalysts coupled easily accessible a wide range of biomass-derived platforms containing aldehyde groups, where a series of functionalized structurally diverse branched benzylic and heterocyclic amines (more than 21 samples) were synthesized in good to excellent yield. The reaction pathways reflected that the metallic Co promoted the imine formation by the activating C=O group of the aldehyde groups, while the acid sites on the particle surface was responsible for the hydrogenation of imine to amine. And also, this protocol could exhibit a similar reactivity during the gram-scale as well as possess a longer lifecycle as it can be easily recycled and reused up to eight times without any significant loss

of catalytic activity and selectivity. The above findings strongly confirm an available and the feasible preparation of simple but highly efficient catalysts towards reductive amination of renewable sources. By and large, the advantages of this newly developed method include operational simplicity, high stability, easily recyclable, cost-effective of the catalyst, and good functional group compatibility for the synthesis of functional amines, as well as the highly efficient and industrial applicable synthesis process.

**Acknowledgment** This work was supported financially by the National Key R&D Program of China (2018YFB1501500, National Natural Science Foundation of China (51976225), DNL Cooperation Fund, and Chinese Academy of Sciences (DNL201916).

**Author contributions** J. G. L. and L. L. M supervised and designed the research. X. Z. Z. performed most of the pre-experiments and data analysis. S. R. Z. performed substrates scope experiments. Z.X.Z. wrote the paper. J.G.L. reviewed and wrote the original manuscript. All authors discussed the results and assisted during manuscript preparation.

**Competing interests** The authors declare no competing financial interests.

**Additional information** Correspondence and requests for materials should be addressed to L. L. M or J. G. L.

## Reference

1. Y. Liao, S.-F. Koelewijn, G. Van den Bossche, J. Van Aelst, S. Van den Bosch, T. Renders, K. Navare, T. Nicolai, K. Van Aelst, M. Maesen, H. Matsushima, J. M. Thevelein, K. Van Acker, B. Lagrain, D. Verboekend and B. F. Sels, *Science*, 2020, **367**, 1385-1390.
2. N. Luo, T. Montini, J. Zhang, P. Fornasiero, E. Fonda, T. Hou, W. Nie, J. Lu, J. Liu, M. Heggen, L. Lin, C. Ma, M. Wang, F. Fan, S. Jin and F. Wang, *Nature Energy*, 2019, **4**, 575-584.
3. E. Hayashi, Y. Yamaguchi, K. Kamata, N. Tsunoda, Y. Kumagai, F. Oba and M. Hara, *J Am Chem Soc*, 2019, **141**, 890-900.
4. N. Zhang, Y. Zou, L. Tao, W. Chen, L. Zhou, Z. Liu, B. Zhou, G. Huang, H. Lin and S. Wang, *Angew Chem Int Edit*, 2019, **58**, 15895-15903.
5. H. Li, S. Yang, S. Saravanamurugan and A. Riisager, *Acs Catalysis*, 2017, **7**, 3010-3029.
6. J. He, L. Chen, S. Liu, K. Song, S. Yang and A. Riisager, *Green Chemistry*, 2020, **22**, 6714-6747.

7. I. Bodachivskiy, U. Kuzhiumparambil and D. B. G. Williams, *Chemsuschem*, 2018, **11**, 642-660.
8. E. C. Gaudino, G. Cravotto, M. Manzoli and S. Tabasso, *Green Chemistry*, 2019, **21**, 1202-1235.
9. S. Chen, R. Wojcieszak, F. Dumeignil, E. Marceau and S. Royer, *Chemical Reviews*, 2018, **118**, 11023-11117.
10. H. Alinezhad, H. Yavari and F. Salehian, *Current Organic Chemistry*, 2015, **19**, 1021-1049.
11. D. Carnevali, O. Guevremont, M. G. Rigamonti, M. Stucchi, F. Cavani and G. S. Patience, *Acs Sustain Chem Eng*, 2018, **6**, 5580-5587.
12. Y. Wang, X. Yang, H. Zheng, X. Li, Y. Zhu and Y. Li, *Molecular Catalysis*, 2019, **463**, 130-139.
13. R. Mariscal, P. Maireles-Torres, M. Ojeda, I. Sadaba and M. Lopez Granados, *Energ Environ Sci*, 2016, **9**, 1144-1189.
14. M. Chatterjee, T. Ishizaka and H. Kawanami, *Green Chemistry*, 2016, **18**, 487-496.
15. S. Gomez, J. A. Peters and T. Maschmeyer, *Adv Synth Catal*, 2002, **344**, 1037-1057.
16. T. Komanoya, T. Kinemura, Y. Kita, K. Kamata and M. Hara, *J Am Chem Soc*, 2017, **139**, 11493-11499.
17. T. Senthamarai, K. Murugesan, J. Schneidewind, N. V. Kalevaru, W. Baumann, H. Neumann, P. C. J. Kamer, M. Beller and R. V. Jagadeesh, *Nat Commun*, 2018, **9**.
18. R. V. Jagadeesh, K. Murugesan, A. S. Alshammari, H. Neumann, M.-M. Pohl, J. Radnik and M. Beller, *Science*, 2017, **358**, 326-+.
19. S. Nishimura, K. Mizuhori and K. Ebitani, *Research on Chemical Intermediates*, 2016, **42**, 19-30.
20. J. J. Martinez, E. Nope, H. Rojas, M. H. Brijaldo, F. Passos and G. Romanelli, *Journal of Molecular Catalysis a-Chemical*, 2014, **392**, 235-240.
21. K. Zhou, B. Chen, X. Zhou, S. Kang, Y. Xu and J. Wei, *Chemcatchem*, 2019, **11**, 5562-5569.
22. M. Manzoli, E. C. Gaudino, G. Cravotto, S. Tabasso, R. B. N. Baig, E. Colacino and R. S. Varma, *Acs Sustain Chem Eng*, 2019, **7**, 5963-5974.
23. L. Yu, D. H. Deng and X. H. Bao, *Angew Chem Int Edit*, 2020, **59**, 15294-15297.
24. D. Deng, L. Yu, X. Chen, G. Wang, L. Jin, X. Pan, J. Deng, G. Sun and X. Bao, *Angewandte Chemie International Edition*, 2013, **52**, 371-375.
25. J. Liu, Y. Zhu, C. Wang, T. Singh, N. Wang, Q. Liu, Z. Cui and L. Ma, *Green Chemistry*, 2020, **22**, 7387-7397.
26. W. Lv, Y. T. Zhu, J. Liu, C. G. Wang, Y. Xu, Q. Zhang, G. Y. Chen and L. L. Ma, *Acs Sustain Chem Eng*, 2019, **7**, 5751-5763.
27. C. G. Lu and J. Liu, *J Phys Chem B*, 2006, **110**, 20254-20257.
28. X. Y. Li, C. M. Zeng, J. Jiang and L. H. Ai, *J Mater Chem A*, 2016, **4**, 7476-7482.
29. X. Sun, A. I. Olivos-Suarez, L. Oar-Arteta, E. Rozhko, D. Osadchii, A. Bavykina, F. Kapteijn and J. Gascon, *Chemcatchem*, 2017, **9**, 1854-1862.
30. K. Murugesan, T. Senthamarai, M. Sohail, A. S. Alshammari, M. M. Pohl, M. Beller and R. V. Jagadeesh, *Chemical Science*, 2018, **9**, 8553-8560.

31. D. Li, Q. Y. Liu, C. H. Zhu, H. Y. Wang, C. H. Cui, C. G. Wang and L. L. Ma, *J Energy Chem*, 2019, **30**, 34-41.
32. Z. L. Yuan, B. Liu, P. Zhou, Z. H. Zhang and Q. Chi, *Journal of Catalysis*, 2019, **370**, 347-356.
33. Y. L. Zhang, X. Z. Lin, X. J. Li, C. G. Wang, Q. Long and L. L. Ma, *New Journal of Chemistry*, 2018, **42**, 15968-15973.
34. X. H. Liu, C. G. Wang, Y. Zhang, Y. Qiao, Y. Pan and L. L. Ma, *Chemsuschem*, 2019, **12**, 4791-4798.
35. X. Z. Zhuang, H. Zhan, Y. Q. Huang, Y. P. Song, X. L. Yin and C. Z. Wu, *Bioresource Technol*, 2018, **267**, 17-29.
36. X. Z. Zhuang, H. Zhan, Y. P. Song, C. He, Y. Q. Huang, X. L. Yin and C. Z. Wu, *Fuel*, 2019, **236**, 960-974.
37. L. Wang, Y. Weng, P. Duan, X. Liu, X. Wang, Y. Zhang, C. Wang, Q. Liu and L. Ma, *SN Applied Sciences*, 2019, **1**, 404.
38. C. H. Zhu, H. Y. Wang, H. Li, B. J. Cai, W. Lv, C. L. Cai, C. G. Wang, L. Yan, Q. Y. Liu and L. L. Ma, *Acs Sustain Chem Eng*, 2019, **7**, 19556-19569.
39. N. S. Gould, H. Landfield, B. Dinkelacker, C. Brady, X. Yang and B. J. Xu, *Chemcatchem*, 2020, **12**, 2106-2115.
40. W. Chen, Y. Sun, J. Du, Z. Si, X. Tang, X. Zeng, L. Lin, S. Liu and T. Lei, *Journal of Chemical Technology and Biotechnology*, 2018, **93**, 3028-3034.
41. W. Wu, W. Zhang, Y. Long, J. H. Qin and J. T. Ma, *Molecular Catalysis*, 2020, **497**, 10.
42. Y. L. Cao, K. K. Liu, C. Wu, H. P. Zhang and Q. Y. Zhang, *Applied Catalysis a-General*, 2020, **592**, 9.
43. G. F. Liang, A. Q. Wang, L. Li, G. Xu, N. Yan and T. Zhang, *Angew Chem Int Edit*, 2017, **56**, 3050-3054.